Nuclear Instruments and Methods in Physics Research A 1061 (2024) 169103

Contents lists available at ScienceDirect

Nuclear Inst. and Methods in Physics Research, A

journal homepage: www.elsevier.com/locate/nima

Full Length Article

Investigation of high resistivity *p*-type FZ silicon diodes after ^{60}Co γ-irradiation ☆

C. Liao [a,*], E. Fretwurst [a], E. Garutti [a], J. Schwandt [a], I. Pintilie [b], A. Nitescu [b], A. Himmerlich [c], M. Moll [c], Y. Gurimskaya [c], Z. Li [d]

[a] Institute for Experimental Physics, University of Hamburg, Hamburg, Germany
[b] National Institute of Materials Physics, Bucharest, Romania
[c] European Organization for Nuclear Research (CERN), Geneva, Switzerland
[d] College of physics and optoelectronic engineering, Ludong University, Yantai, China

ARTICLE INFO

Keywords:
^{60}Co γ-rays
FZ p-type silicon
Radiation damage
B_iO_i
C_iO_i
TSC
DLTS
Surface current

ABSTRACT

In this work, the effects of ^{60}Co γ-ray irradiation on high resistivity *p*-type diodes have been investigated. The diodes were exposed to dose values of 0.1, 0.2, 1, and 2 MGy. Both macroscopic (I–V, C–V) and microscopic investigations, by means of Thermally Stimulated Current (TSC) and Deep Level Transient Spectroscopy (DLTS) techniques, were conducted to characterize the radiation-induced changes. The investigated diodes were manufactured on high resistivity *p*-type Float Zone (FZ) silicon and were further classified into two types based on the isolation technique between the pad and guard ring: *p*-stop and *p*-spray. After irradiation, the macroscopic results of current–voltage and capacitance–voltage measurements were obtained and compared with existing literature data. Additionally, the microscopic measurements focused on the development of the concentration of different radiation-induced defects, including the Boron interstitial-Oxygen interstitial (B_iO_i) complex, the Carbon interstitial-Oxygen interstitial (C_iO_i) defect, the H40K, and the so-called I_P^*.

To investigate the thermal stability of induced defects in the bulk, isochronal annealing studies were performed in the temperature range of 100 °C to 300 °C. These annealing processes were carried out on diodes irradiated with doses of 1 and 2 MGy. Furthermore, in order to investigate the unexpected results observed in the C–V measurements after irradiation with high dose values, the surface conductance between the pad and guard ring was measured as a function of both dose and annealing temperature.

1. Introduction

In High Luminosity Large Hadron Collider (HL-LHC) experiments, strip and pixel silicon sensors in the inner tracking detectors have to cope with extraordinarily high particle rates due to up to 200 p–p collisions per bunch crossing. New types of sensors to be used for this purpose, started to be developed. They are manufactured on boron doped (*p*-type) silicon and have different structures, from the simplest *p-i-n* diode to devices which amplifies the signals and have better time resolution, as e.g. the Low Gain Avalanche Detectors (LGADs) [1–4]. The degradation in the performance of these sensors is caused by the generation of electrically active radiation-induced defects. For instance, the charged defects at room temperature (e.g. E30K, B_iO_i, H140K, H152K and I_P) [5–8] cause changes of the space charge density (N_{eff}). Vacancy related traps such as V_2 and V_3 [9] lead to the degradation of charge collection efficiency (CCE) and an increase of dark current. In general, the radiation-induced defects can be classified according to their size: point defects, up to 2–3 atoms size, or more extended ones, also known as cluster-related defects. All the radiation-induced defects contribute to the degradation of silicon sensors and can be characterized using spectroscopic techniques such as Deep Level Transient Spectroscopy (DLTS), for low defect concentration, and Thermally Stimulated Current (TSC) after high levels of irradiation when DLTS is not applicable anymore. During a temperature scan, both, point and cluster-related defects are contributing to the signals observed in TSC and DLTS measurements. Separating and analyzing the combined effects of these defects pose a challenge for these techniques.

The main radiation damage effect seen in *p*-type silicon sensors is the deactivation of the boron dopant. Thus, the atoms of substitutional Boron (B_s) may switch the sites with interstitial silicon (Si_i) created

☆ Work performed in the frame of the CERN-RD50 collaboration.

* Corresponding author.
E-mail addresses: chuan.liao@desy.de (C. Liao), ioana@infim.ro (I. Pintilie).

https://doi.org/10.1016/j.nima.2024.169103
Received 18 September 2023; Received in revised form 22 December 2023; Accepted 10 January 2024
Available online 13 January 2024

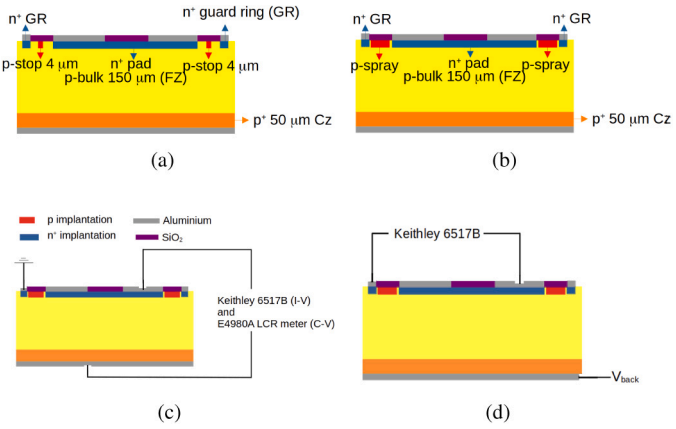

Fig. 1. (a) Side view of *p*-stop diodes. (b) Side view of *p*-spray diodes. (c) Schematic representation of the electrical setup used for *I–V*/*C–V* measurements. (d) Schematic representation of the electrical circuit used for measuring the surface current.

during radiation via a Watkins replacement mechanism [10] and transform in Boron interstitial (B_i), losing its acceptor character. The B_i atoms migrate in the crystal and react with interstitial Oxygen, found in abundance in silicon, leading to the formation of B_iO_i complex. Another possible acceptor removal mechanism in *p*-type silicon considers the interaction between the negatively charged acceptor dopant (B_s for boron-doped silicon) and the positively charged Si_i atoms forming the B_s-Si_i complex [11,12]. The boron removal effect induced by 23 GeV protons, 5.5 MeV electrons and 1 MeV neutrons was investigated in the framework of the CERN-RD50 "Acceptor removal project" [13–17]. This effect can also be introduced by high-energy photons i.e. ^{60}Co γ-rays [18–20]. While hadrons can produce both point and cluster-related defects, γ-rays introduce only point defects [21,22]. In this work, n^+-*p* diodes irradiated with ^{60}Co γ-rays are investigated. This means that the changes in the macroscopic properties of silicon sensors, as determined from Current–Voltage (*I–V*) or Capacitance–Voltage (*C–V*) characteristics are attributed to point defects only.

The paper is structured as follows. Section 2 includes information on the fabrication of the investigated diodes, irradiation details and measurement procedures. In Section 3 the results of the macroscopic (*I–V*/*C–V*) and microscopic (TSC) investigations, on as-irradiated and annealed samples, are presented and discussed. The conclusions of this work are presented in Section 4.

2. Experimental details

The study was performed on 12 *p*-type silicon diodes which were designed for upgrading the planar pixel sensors in the Compact Muon Solenoid (CMS) inner tracker for HL-LHC at CERN. These diodes were manufactured by Hamamatsu Photonics K. K. (HPK) [23], and were processed on, so-called, FDB150 (float zone Si–Si direct bonded) wafers, obtained by bonding together two wafers: a high resistivity float zone (FZ) wafer and a low resistivity handle one, produced with the Czochralski (Cz) method. The FZ wafer is thinned down to an active thickness of 150 μm and after processing the pixel sensors, diodes and other test structures, the handle wafer is thinned down to 50 μm, resulting in a total thickness of 200 μm—see Fig. 1.

The initial resistivity of the FZ bulk is 4 kΩ cm, corresponding to a boron doping of about $N_{eff,0} = 3.5 \times 10^{12}$ cm^{-3}. Besides boron, the main impurity in the bulk is oxygen, having a concentration of about 1×10^{17} cm^{-3} [24]. The backside Cz material has a boron content of 1×10^{19} cm^{-3}. According to the design of the isolation between the pad and guard ring structure, there are two types of diodes: with *p*-stop (FDB150P, simplified to F150P in this work) and *p*-spray (FDB150Y, simplified to F150Y in this work). The pad and guard ring are isolated by a thin (≈4 μm) boron-implanted region on the surface in the case of *p*-stop, while *p*-spray has a boron implant across the full wafer surface before the processing of the sensors (see Fig. 1(a) and Fig. 1(b)). The active area of the diodes is 0.25 cm^2. More details can be found in [24,25].

Table 1
Device information.

p-stop1	F150P-1	F150P-3	F150P-5	F150P-8
p-stop2	F150P-2	F150P-4	F150P-7	F150P-9
p-spray	F150Y-1	F150Y-2	F150Y-5	F150Y-8
Dose value (kGy)	94 ± 0.96	189 ± 3.9	924 ± 27	1861 ± 56

The 12 diodes were divided into four groups, each containing two *p*-stop type and one *p*-spray type diode. The proposed dose values for ^{60}Co γ irradiation of each of the groups were 0.1, 0.2, 1 and 2 MGy. The irradiation was performed using the ^{60}Co Panoramic Irradiation facility at Rudjer Boskovic Institute [26]. Considering the radiation flux and exposure time, the following dose values in Silicon were achieved: 94 ± 0.96, 189 ± 3.9, 924 ± 27 and 1861 ± 56 kGy. The investigated diodes and the achieved irradiation doses are given in Table 1.

The electrical performance of the diodes was measured by means of *I–V* and *C–V* characteristics at 20 ± 0.01 °C. For all the diodes, the space charge density (N_{eff}) and the depleted depth $w(V)$ as a function of voltage V were determined from *C–V* measurements corresponding to a frequency of 500 kHz and an AC voltage of 500 mV. The electrical circuit for measuring *I–V*/*C–V* characteristics is depicted in Fig. 1(c). The current flow between the pad and the guarding was measured using the circuit given in Fig. 1(d). The radiation-induced electrically active defects were investigated by means of the TSC technique. Details of the experimental setup can be found in [14,22,27,28]. In this work, the trap filling was performed at different filling temperatures (T_{fill} = 10–100 K, in steps of 10 K) by injection of a forward current (I_{fill}) produced by a forward bias of V_{fill} = 10 V for 30 s. For T_{fill} = 10 K, the I_{fill} is slightly less than 1 mA and shows negligible dependence on the dose and the type of isolation. For $T_{fill} \geq 20$ K, all the I_{fill} were roughly equal to 1 mA. The TSC spectra were then recorded for different reverse biases V_{bias} applied to the sample (−100 to −300 V in steps of 50 V) during heating up the samples with a constant heating rate of β = 0.183 K/s. Direct measurements of the capture cross sections for electrons and holes of some newly detected defects, with energy levels close to the midgap of silicon, have been performed using the DLTS technique [17]. The measurements were performed at 270 K, where the DLTS specific requirements for accurate evaluations are fulfilled. Isochronal annealing experiments were conducted using a Thermo SCIENTIFIC oven [29] in ambient atmosphere.

3. Results and discussion

3.1. As-irradiated devices

In Fig. 2 are given the *I–V* and the $1/C^2$–*V* curves of all *p*-spray diodes irradiated to different dose values. Included are also the data for the F150Y-8 diode before being irradiated. The N_{eff} depth profile was determined from *C–V* measurements, considering the following relations for $N_{eff}(w(V))$ and the depletion depth $w(V)$:

$$N_{eff}(V) = \frac{2}{\epsilon_0 \epsilon_r A^2 q_0 \, d(1/C^2)/dV} \quad (1)$$

$$w(V) = \frac{\epsilon_0 \epsilon_r A}{C(V)} \quad (2)$$

where C is the measured capacitance, ϵ_0 is the permittivity of vacuum, ϵ_r the relative permittivity of silicon (11.9), q_0 is the elementary charge, A is the active pad area. Considering the voltage dependence of the depletion depth (Eq. (2)) the current density $j_d(V)$ can be calculated from the measured *I–V* curves according to $j_d(V) = I(V)/(A \cdot w(V))$.

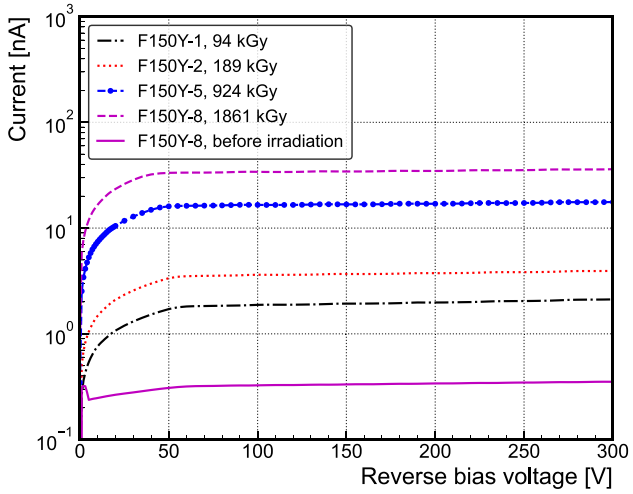

(a)

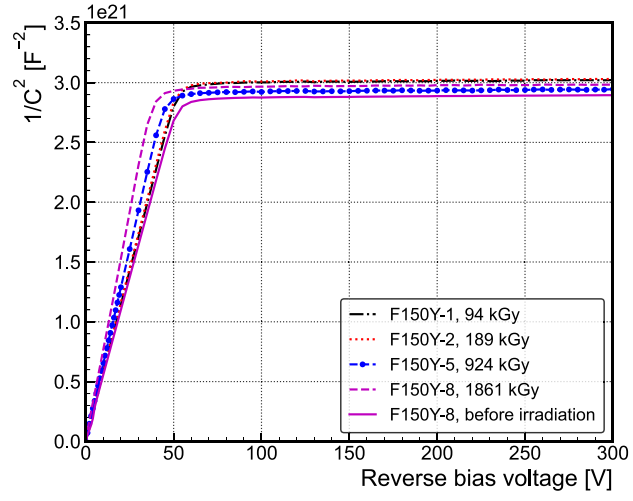

(b)

Fig. 2. (a) Current–voltage (I–V) characteristics of p-spray diodes irradiated to different dose values (see legend). (b) Capacitance–voltage ($1/C^2$–V) characteristics for the same diodes as in (a) for a frequency f = 500 kHz. Included in (a) and (b) are data for one diode before irradiation. Measurement condition: T = 20 °C, humidity ≤ 10%.

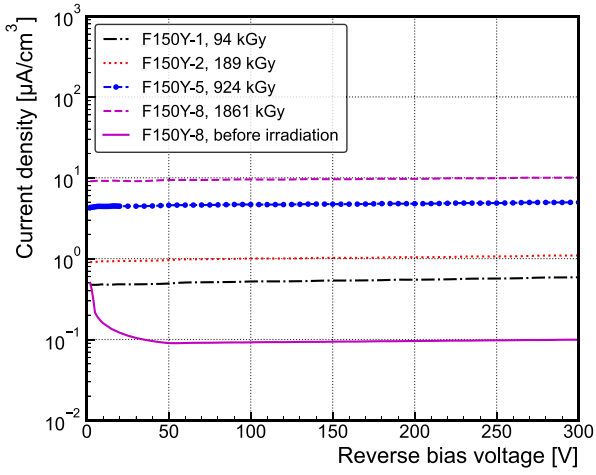

(a)

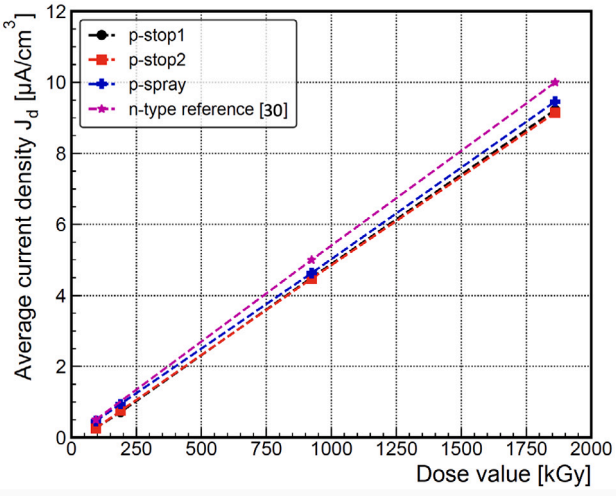

(b)

Fig. 3. (a) Density of leakage current (j_d) versus bias voltage V, which was developed from Figs. 2(a) and 2(b). (b) Average current density J_d vs. dose value. The values were taken from (a) in the voltage range from 100 V to 150 V (more details see text).

The results are shown in Fig. 3(a), for the different dose values applied to the corresponding p-spray diodes. Average current densities J_d as taken from $j_d(V)$ data, in the 100 V and 150 V voltage range for V_{bias}, are plotted in Fig. 3(b) as a function of the dose, for both, p-stop and p-spray diodes. The data achieved for n-type oxygen-enriched DOFZ diodes, taken from Ref. [30], are also included. As can be observed in Fig. 3(b), all the presented results are nearly identical.

For the average current density J_d of the p-spray type diodes, an error of 1% was estimated. This includes the uncertainty of the measured current and the depleted volume extracted from the C–V data. The corresponding value for the p-stop diodes was estimated to be 2%. The definition of the current-related damage parameters α can also be applied to γ-ray damage with dose value (D):

$$\alpha_\gamma = \frac{\Delta J_d}{\Delta D} \tag{3}$$

According to Eq. (3) the α_γ value for the p-spray diodes is estimated to be $\alpha_\gamma = 5.09 \times 10^{-12}$ A/(Gy cm^3) with an error of 4.4%, and for the p-stop diodes it is 5.07×10^{-12} A/(Gy cm^3) with an error of 5.4%. The errors are dominated by the uncertainties of the dose values (see Table 1). Fig. 4 presents the extracted N_{eff} profiles for p-spray diodes, of different irradiation dose values. With increasing the dose, the profiles are shifted to lower N_{eff} values. Such a behavior is expected due to the deactivation of the initial boron concentration caused by irradiation, the so-called acceptor removal effect [13–17].

It should be mentioned here that the C–V measurements were also performed for different frequencies (230 Hz, 455 Hz, 1 kHz, 10 kHz, 100 kHz, 200 kHz, 400 kHz, 500 kHz) and a frequency dependence was observed only for p-stop diodes. This aspect will be discussed later in Section 3.3 surface effects.

In order to investigate the radiation-induced defect complexes by ^{60}Co γ-rays in the high resistivity FZ diodes, the TSC method is used. Figs. 5(a) and 5(b) show TSC spectra of p-stop and p-spray diodes irradiated to different dose values, respectively. All spectra in Fig. 5 were measured on fully depleted sensors ($V_{\text{bias}} = -200$ V, $V_{\text{dep}} = -50$ V) over the entire TSC temperature range. As can be seen in Fig. 5(a) and Fig. 5(b), several peaks are induced after irradiation and increase with dose. Some of these traps corresponded to the previously detected

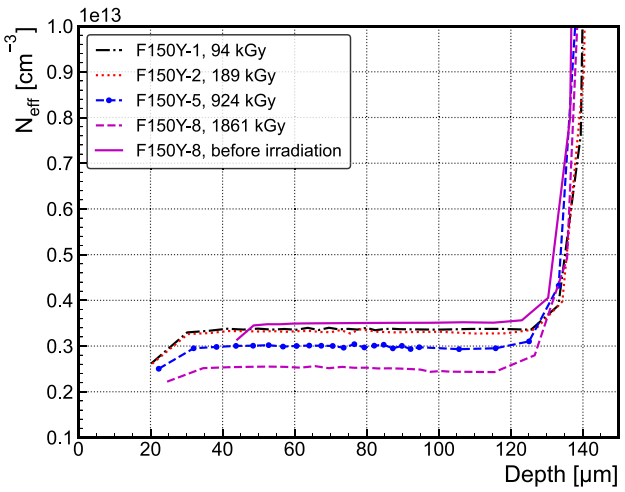

Fig. 4. N_{eff} profile of the *p*-spray diodes for different dose values. The data were evaluated from *C*–*V* measurements performed with a frequency of 500 kHz, by using Eqs. (1) and (2).

radiation-induced defect complexes H40K [7,31,32], VO [33], B_iO_i [5], C_iO_i [22,33] and V_2 [9]. A TSC peak, similar to the one labeled as I_P^* in Fig. 5, has been reported as I_P defect in previous studies and associated with a V_2O complex, a defect generated via a second order process in oxygen-lean material, thermally stable up to 350 °C and with a strong impact on both, the leakage current and N_{eff} [8,34–36]. However, the trapping parameters determined for the I_P^* defect are different compared with of I_P defect as it will shown later on. Accordingly, also the impact of the I_P^* defect on both leakage current and N_{eff} are negligible. By comparing Figs. 5(a) and 5(b), it can be observed that some of the peaks observed in the *p*-spray diodes are smaller compared to those recorded in the *p*-stop ones (H40K, E50K, VO and C_iO_i). This might be due to the different filling of the defects at 10 K. As demonstrated in Fig. 5(c) most peaks show a strong dependence on the filling temperature, except the B_iO_i and I_P^* traps. Previous studies have shown that for the C_iO_i defect an extremely strong dependence on the filling temperature (T_{fill}) exists and thus, suggesting a multi-phonon capture process [22,37]. To get the full defect concentration TSC measurements with different T_{fill} (from 20–100 K in steps of 10 K) were performed.

As can be seen in Fig. 5(c), an increase of the peak height with increasing T_{fill} is not only observed for the C_iO_i defect but also for the H40K, VO and the V_2 defect complexes. Only the B_iO_i and I_P^* have the same peak maximum for different T_{fill}. In the fully depleted diodes, the general formula of thermally stimulated current $I^e_{TSC}(T)$ or $I^h_{TSC}(T)$ for a single electron or hole trap is given by [22,27,28,38,39]:

$$I^e_{TSC}(T) = \frac{1}{2} \cdot q_0 \cdot A \cdot d \cdot e_n(T) \cdot n_t(T_{fill}) \cdot f(T) \quad (4)$$

$$I^h_{TSC}(T) = \frac{1}{2} \cdot q_0 \cdot A \cdot d \cdot e_h(T) \cdot p_t(T_{fill}) \cdot f(T) \quad (5)$$

$$e_{n,p} = \sigma_{n,p} \cdot v_{th,n,p} \cdot N_{C,V} \cdot \exp\left(-\frac{E_a}{k_B T}\right) \quad (6)$$

$$f(T) = \exp\left(-\frac{1}{\beta}\int_{T_0}^{T} \left(e_n(T') + e_p(T')\right) dT'\right) \quad (7)$$

where T is the measured temperature, d is the fully depleted depth. e_n and e_p are the emission rates for electrons and holes. $v_{th,n,p}$ and $N_{C,V}$ are the thermal velocity of electrons/holes and the density of states in the conduction/valence band, respectively, both taken from [40]. The activation energy is defined as $E_a = E_C - E_t$ or $E_a = E_t - E_V$ according to the type of emitted charge, electrons or holes, respectively, with E_t being the energy level of the trap and $E_{C,V}$ the conduction/valence band edges. The $\sigma_{n,p}$ terms stand for the capture cross-section of electrons/holes, k_B is the Boltzmann constant and the $f(T)$ function is the defect occupancy at temperature T. The $n_t(T_{fill})$ and $p_t(T_{fill})$ terms represent the density of defects that are filled with electrons or holes after injection at temperature T_{fill}. The considered capture cross sections for the known defects were taken from the following references (H40K [31], E50K [22], VO [41], B_iO_i [17], C_iO_i [33], V_2 [22], H220K [22]) and kept fixed in the peak fitting procedure.

It should be mentioned here that the feedback activation energy E_a is slightly different compared to reference values (below 5%).

In order to get accurate capture cross-sections for the I_P^* defect in comparison to the previously published data of the I_P defect, measurements have been performed at the National Institute for Material Physics (Bucharest, Romania) using the Deep Level Transient Fourier Spectroscopy (DLTFS) method [42]. Especially direct capture measurements of electrons or holes in the traps are taken via the DLTFS signal amplitude as a function of the trap filling pulse duration t_p at a constant temperature of 270 K. From the recorded curve, which can be represented by the function $Amp(t_p) = Amp \cdot (1 - \exp(t_p/\tau_c))$, the difference $Amp - Amp(t_p)$ is evaluated and the logarithm is plotted versus t_p as shown for electron capture (σ_n) in Fig. 6(a). In this case, the pulse voltage is $U_p = 1$ V (forward injection) and the reverse bias $U_r = -10$ V. Fig. 6(b) shows the results for hole capture (σ_p) of the same I_P^* defect. This measurement is performed with a double pulse sequence: 1st with a 20 μs forward pulse injection at 1 V followed by a second one with −0.1 V of different duration. A linear fit to the data results in the capture time constant τ_c where $1/\tau_c$ is proportional to the capture cross-section for electrons σ_n or holes σ_p, respectively. An activation energy of 0.53 eV from the conduction band of silicon was then determined as the I_P^* defect, by analyzing the transients corresponding to the emission of electrons and accounting for the measured value of σ_n. These values are summarized for the defect I_P^* in Table 2 together with the data for the I_P defect presented in Refs. [34,35].

Table 2
Trapping parameter of I_P^* and I_P.

label	I_P^* (this work)	$I_P^{0/-}$ [34,35]
σ_p (10^{-15} cm^2)	0.02	90
σ_n (10^{-15} cm^2)	7.08	1.7
E_a (eV)	0.53(E_C–E_t)	0.54(E_C–E_t)

For describing the leakage current, I_{LC} measured at temperatures $T \geq 230$ K, the following equation is used [43]:

$$I_{LC} = \chi \cdot T^2 \cdot \exp\left(-\frac{\delta E}{k_B T}\right) \quad (8)$$

where the χ and δE are free parameters in the fitting procedure. The extracted values are achieved from fits to the data in the temperature ranges from 230 K to 250 K at $V_{bias} = -200$ V, which are included in Table 3. For both parameters, the errors were estimated to be below 1%.

The concentrations of defects were determined by fitting the measured TSC peaks using Eqs. (4)–(7). An example of fitting a TSC spectrum is presented in Fig. 5(d) for a *p*-spray diode irradiated with a dose of 924 kGy. The dependence of the C_iO_i concentration ($[C_iO_i]$) on the filling temperature T_{fill} is shown in Fig. 7. As it can be observed, $[C_iO_i]$ initially increases with T_{fill} and saturates at $T_{fill} \geq 60$ K. To describe the T_{fill} dependence of $[C_iO_i]$ the following equation is used [22,37,44]:

$$p_t(T_{fill}) = N_{offset} + P_t \times \frac{1}{1 + a \cdot \exp\left(\frac{E_s}{k_B T_{fill}}\right)} \quad (9)$$

The offset value is caused by the background current. P_t is the total C_iO_i concentration $[C_iO_i]$, and a is a constant. E_s is the activation energy for non-radiative multi-phonon capture of a charge carrier, accounting for the temperature dependence of the capture cross sections [44].

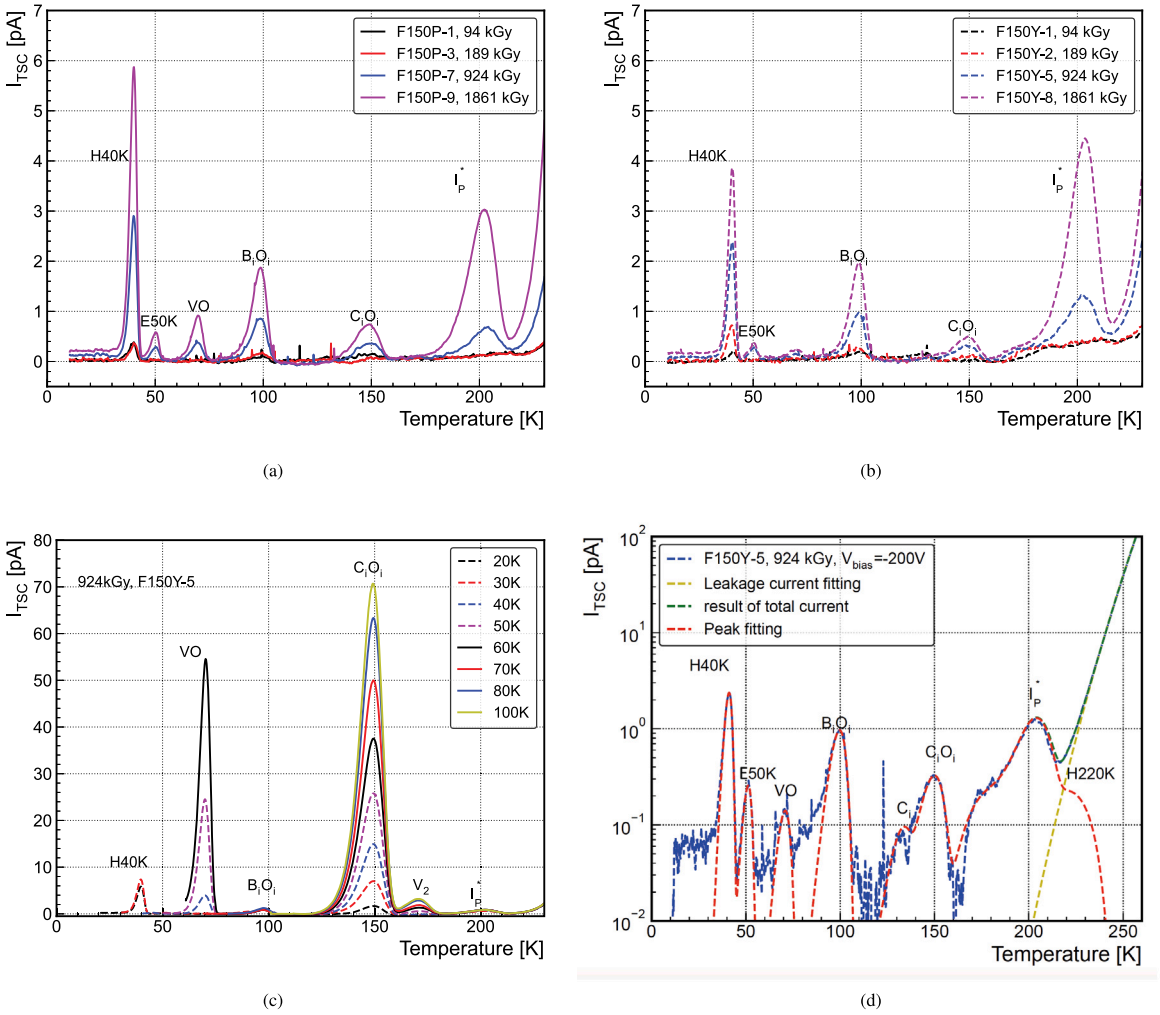

Fig. 5. TSC spectra: (a) for *p*-stop diodes and (b) for *p*-spray diodes. In both cases, the spectra were recorded during applying a reverse bias V_{bias} = −200 V and after filling the traps by injecting a 1 mA forward current (V_{fill} = 10 V) at 10 K. (c) TSC spectra of diode F150Y-5 after the same filling procedure as in (a) and (b), but with different T_{fill} for diode F150Y-5. (d) experimental and computed spectra by fitting the different peaks for diode F150Y-5.

Table 3
Extracted fit parameters for the leakage current LC (V_{bias} = −200 V) by using Eq. (8)

	F150P-1 (94 kGy)	F150P-3 (189 kGy)	F150P-7 (924 kGy)	F150P-8 (1861 kGy)
p-stop χ (A/K)	0.0021	0.0204	0.1273	0.4415
p-stop δE (eV)	0.6594	0.7103	0.7103	0.7196
	F150Y-1 (94 kGy)	F150Y-2 (189 kGy)	F150Y-5 (924 kGy)	F150Y-8 (1861 kGy)
p-spray χ (A/K)	0.0005	0.0037	0.1260	0.2002
p-spray δE (eV)	0.6410	0.6744	0.7103	0.7103

Table 4
Introduction rates.

Defect	H40K	E50K	VO	B_iO_i	C_iO_i	V_2
Introduction rate ($cm^{-3}Gy^{-1}$)	5.2×10^5	1.1×10^4	6.5×10^6	2.5×10^5	1.9×10^7	1.0×10^6

The term $a \cdot \exp\left(\frac{E_s}{k_B T_{fill}}\right)$ is given by the ratio $\frac{n \cdot c_n}{p \cdot c_p}$, where n and p are the concentrations of free electrons and holes under forward bias injection and $c_{n,p}$ are the capture coefficients of the corresponding charge carriers.

The parameters obtained for fitting the C_iO_i data in Fig. 7 are: a = (1.18 ± 0.03) ×10^{-2}, E_s = (13.2 ± 0.2) meV, N_{offset} = (6.1 ± 0.5) × 10^{10} cm^{-3}, and N_t = (2.5 ± 0.1) ×10^{12} cm^{-3}. The result of the fit is plotted in Fig. 7 together with the experimental data. We also included a calculated curve using the values of $a = 10^{-4}$ and E_s = 37.3 meV given in a previous study on neutron irradiated diodes [22], considering the same values of N_{offset} and N_t as in our data fit. The different a and E_s values in our fit compared with those from Ref. [22] might be explained by the potential barriers surrounding the clustered regions induced by neutron irradiation, which can slow down the carrier capturing processes [45,46].

The increase with dose in the concentration of the TSC detected defects of the *p*-spray diodes are shown in Fig. 8. Worth noting is that among all the defects, only the I_P^* defect does not have a linear

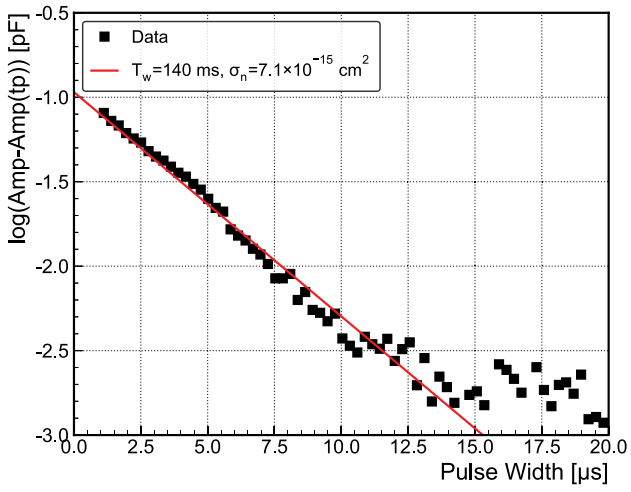

(a)

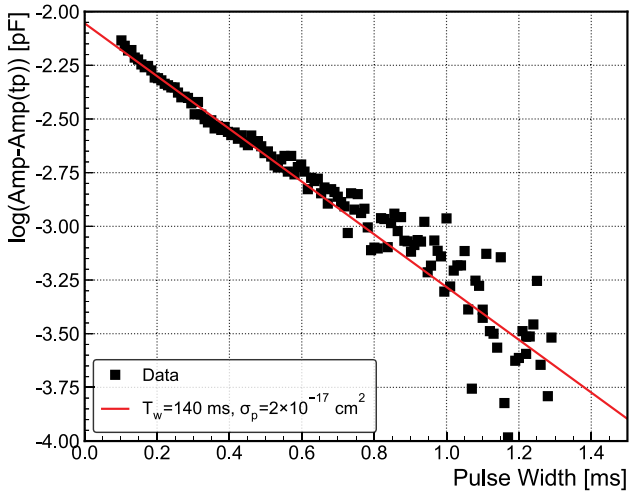

(b)

Fig. 6. Direct measurements of the capture cross sections of the I_P^* defect, performed on sample F150Y-5 at 270 K. (a) Amplitude difference versus pulse width t_p for electron capture σ_n. (b) Amplitude difference versus t_p for hole capture σ_p. The measurement conditions and procedures are given in the text.

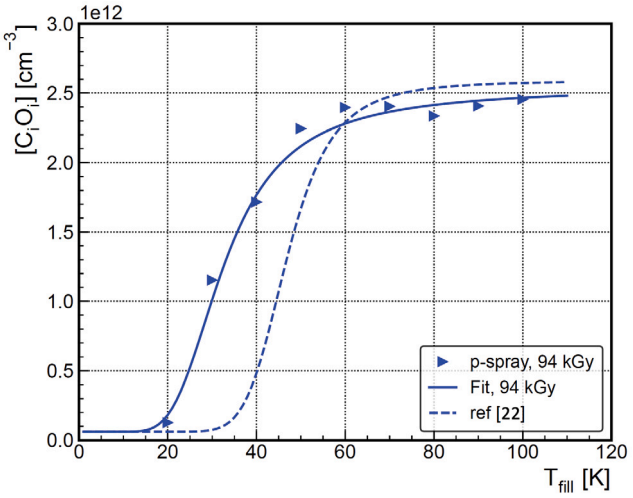

Fig. 7. C_iO_i concentration as a function of the filling temperature T_{fill}. The data are extracted from the TSC spectra of F150Y-1. The solid line is a fit to the data according to Eq. (9), the parameters for the dotted curve are taken from Ref. [22].

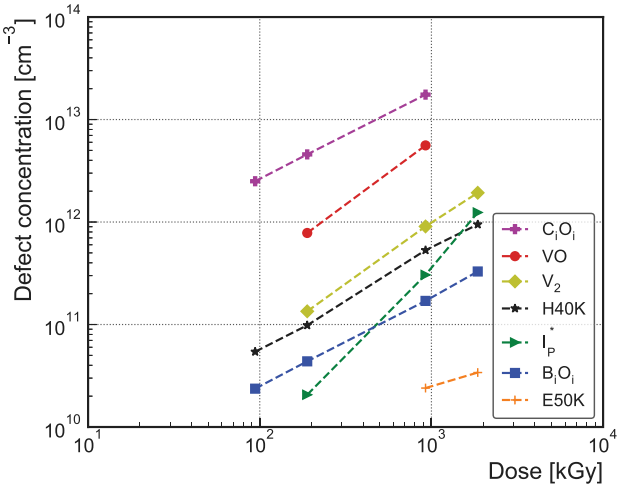

Fig. 8. Defect concentration vs. Dose value included all observed defects.

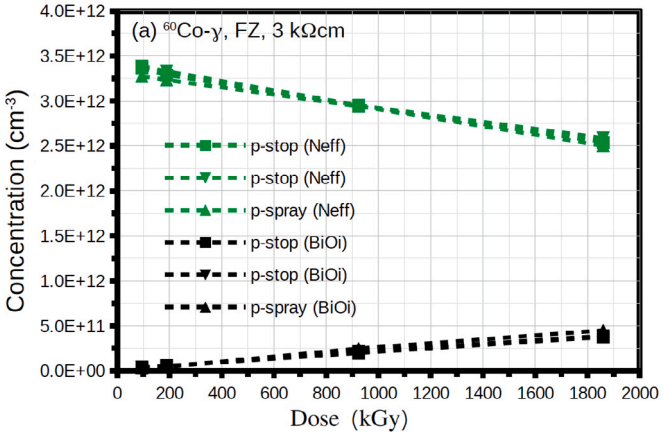

Fig. 9. Dose dependencies of N_{eff} and B_iO_i concentration in all the investigated diodes.

dependence on dose, but a quadratic one (slope ≈ 2 in Fig. 8) as previously reported for the I_P defect, a radiation-induced defect formed via a second order process. Considering the definition of the introduction rate $g = \frac{\Delta N_t}{\Delta D}$, the rates for γ-ray irradiation were extracted from the linear fits to the data (see Fig. 8) and are summarized in Table 4.

The variation of N_{eff} with increasing the dose is given in Fig. 9 along with the corresponding concentration of B_iO_i defect. It is worth noting that the loss in N_{eff} is about twice the increase in the concentration of B_iO_i defect. This is an evidence that for the high resistivity samples investigated here the loss seen in N_{eff} with increasing the dose is due to the formation of B_iO_i donors

It should be mentioned here that the errors in the extracted defect concentrations are caused by different reasons:

(a) The fitting procedure of the peak maxima leads to about 2% error in the determined defect concentration.

(b) Errors of about 3% are estimated for calculating the $n_t(T_{fill})/N_t$ fraction of filled defects at low temperature by forward current injection, due to the filling temperature dependence of H40K, C_iO_i and V_2.

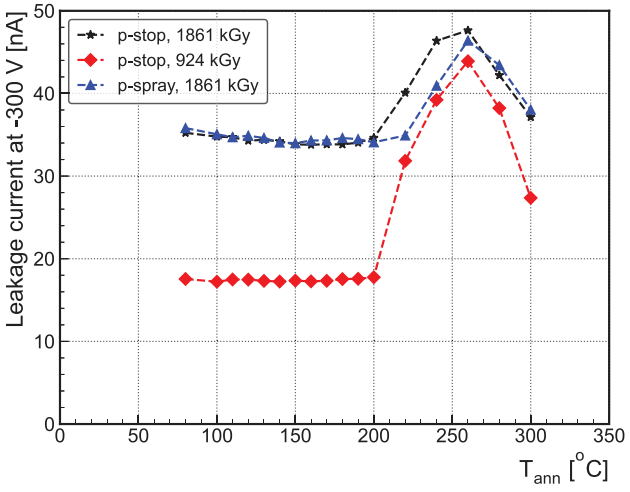

Fig. 10. The development of leakage current measured at room temperature and $V = -300$ V with annealing temperature.

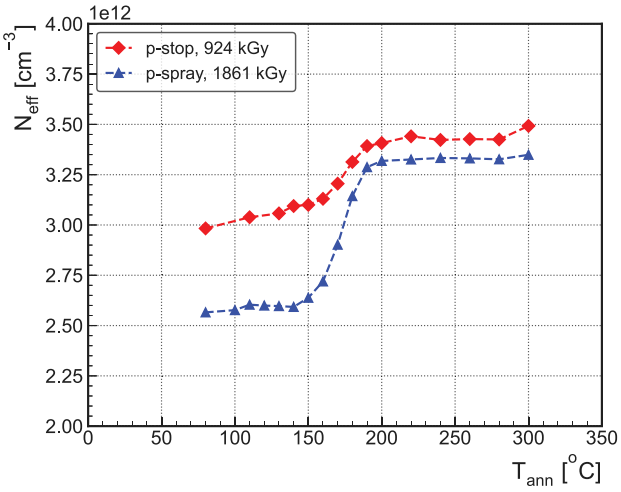

Fig. 11. Extracted N_{eff} from C–V measurement at room temperature as a function of annealing temperature.

(c) The noise of the TSC signal contributes to an error in the determined defect concentration of about 2%.

Assuming all errors to be uncorrelated, the total error on the defect concentration is below 5%.

3.2. Annealing studies

Two *p*-stop diodes, F150P-7 and F150P-8, and one *p*-spray diode F150Y-8 have been subjected to annealing experiments and the changes in the macroscopic and microscopic properties of these diodes have been studied.

Isochronal annealing experiments have been performed for 15 min at different temperatures, between 100 °C and 300 °C. The temperature was increased in steps of 10 °C for annealing up to 200 °C and in steps of 20 °C in the higher temperature range. The annealing behavior of the reverse current at −300 V is plotted in Fig. 10 for the three annealed irradiated diodes. As can be seen, while the change of the leakage current for $T_{ann} \leq 200$ °C is very small, it becomes significant for higher temperatures for all the diodes. A sudden increase of the leakage current takes place in the 200–260 °C temperature range, being followed by a sharp decrease for higher temperatures. The reason for this sudden change is not clear yet.

The development of N_{eff} with annealing temperature is presented in Fig. 11. The given N_{eff} data represents the average values determined from the $N_{eff}(w)$ profiles in the 60 µm and 100 µm depth range. Between 150 °C and 200 °C the N_{eff} increases, recovering most of the initial doping value of non-irradiated devices (3.5×10^{12} cm^{-3}), e.g. 98% for F150P-7 and 95% for F150Y-8. This recovery of the acceptor doping is related to the dissociation of the B_iO_i defect which anneals out in the 150–200 °C temperature range [5,10,14,47,48]. Thus, the initial doping values in the investigated high resistivity samples are almost fully recovered after annealing at temperatures above 150 °C. On the other hand, for similar heat treatments, the full recovery of the initial doping does not occurs in the gain layer of LGADs [49]. The main difference between our PAD diodes and the gain layers in LGADS is the level of Boron doping. In the gain layer of LGADs the Boron doping is much larger, of 1×10^{16} atoms/cm^3 compared with 1×10^{12} atoms/cm^3 in the samples investigated here. Thus, if by dissociation of B_iO_i in low doped diodes, the Bi has a free path to return on a substitutional position, in the gain layer of LGADs the path of returning is not anymore so free, Boron–Boron reactions becoming possible, forming e.g. B_iB_s defect (not electrically active) and stable at high temperatures. In our opinion, such a reaction path involving Boron atoms, can explain the weaker recovery in LGADs compared with high resistivity diodes.

The TSC spectra recorded on the diode F150P-8 after annealing at different temperatures are given in Fig. 12(a) and Fig. 12(b). As it can be seen while H40K anneals out at 120 °C, B_iO_i and I_p^* defects starts to anneal out at 160 °C and are disappearing after the treatment at 200 °C. Worth noting is the significantly lower thermal stability of the I_p * defect compared with the previously reported one for the I_p defect in [36]. Thus, although both defects show a quadratic dose dependence, there are significant differences between them concerning trapping parameters (see Table 2) and thermal stability, indicating that they are different structural point defects. The dominant C_iO_i defect is stable in all the studied temperature ranges.

A further interesting observation is, that the decrease in the concentration of B_iO_i and I_p^* defects are accompanied by the formation of another center (*defect1*) and its concentration is growing up to about 200 °C (see Fig. 12(a)). After dissociation of B_iO_i defect, boron atom return on the substitutional site (B_s) and is recovering its acceptor character. This process is reflected in an increase of N_{eff} with twice the amount of the dissociated B_iO_i donor. For the *p*-spray diode, the variation in the N_{eff} given in Fig. 11 is $[\Delta N_{eff}] = 7.25 \times 10^{11}$ cm^{-3} (between 140 °C and 200 °C). The total amount of dissociated B_iO_i defect for the same sample is $[B_iO_i] = 3.5 \times 10^{11}$ cm^{-3} (see Fig. 13(b)), almost a half of $[\Delta N_{eff}]$. Because the initial boron doping is mostly restored during the dissociation of B_iO_i defect and considering the concentration of the newly formed *defect1* (of 4.2×10^{11} cm^{-3}), we conclude that the boron atom is most probably not part of *defect1*.

The *defect1* is stable up to about 240 °C (see Fig. 12(b)) and then starts to transform into the *defect2* up to the limit of the used oven (300 °C). The variation in defect concentration is given in Fig. 13(a) and Fig. 13(b). From TSC experiments with different applied bias voltages, no change in the position of the peak is found for defects 1 and 2. Also, no change in the N_{eff} values are determined during the annealing transformations occurring between 200 °C and 300 °C. This indicates that both defects (1 and 2) are in a neutral charge state at room temperature. In addition, experiments for 0 V filling at $T_{fill} = 20$ K and 40 K were performed. *defect1* and *defect2* are both detected in this way (see Fig. 14), evidencing that they are acting as traps for holes.

3.3. Surface effect

Contrary to the investigated *p*-spray diodes, the *p*-stop devices after high dose values (1 MGy and 2 MGy) show a frequency dependence of the C–V characteristics, an important source of errors when estimating N_{eff} depth profiles. This was shown previously for the 230 Hz–10 kHz frequency range [19,20]. As we will show further, the phenomena

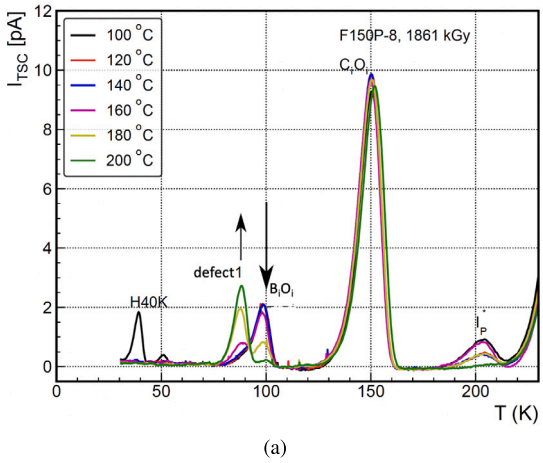

(a)

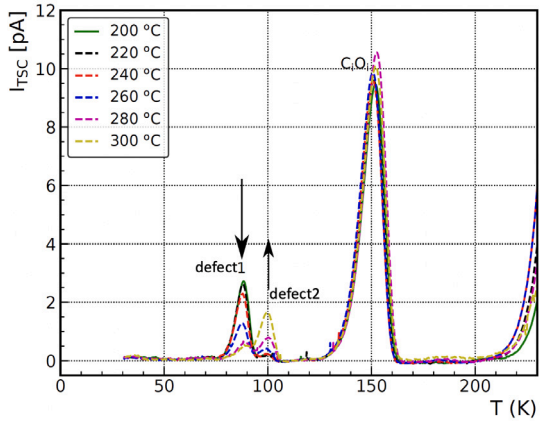

(b)

Fig. 12. (a) TSC spectra for diode F150P-8 after isochronal annealing from 100 °C to 200 °C. (b) TSC spectra for diode F150P-8 after isochronal annealing from 200 °C to 300 °C. Measurement details for (a) and (b): Trap filling by forward current (I_{fill} = 1 mA) injection at T_{fill} = 30 K. The diode was irradiated with ^{60}Co-γ to a dose value of about D = 2 MGy, and the bias voltage during the temperature scan was V_{bias} = −300 V.

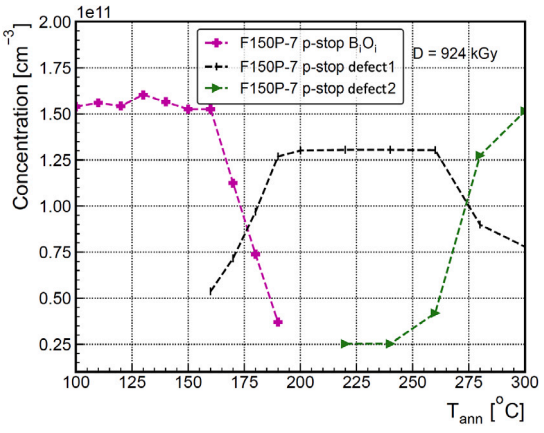

(a)

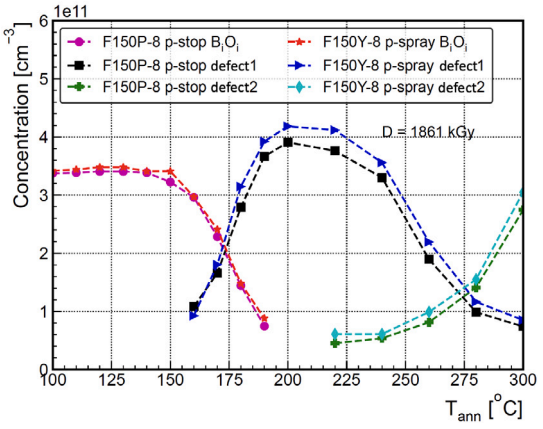

(b)

Fig. 13. (a) Evolution of the defects (B_iO_i, Peak 1 and Peak 2) concentrations in diode F150P-7 as a function of annealing temperature T_{ann}. (b) Evolution of the defects (B_iO_i, Peak 1 and Peak 2) concentrations in diodes F150P-8 and F150Y-8 as a function of annealing temperature T_{ann}. Both (a) and (b) are determined from TSC measurements in the temperature range of 70 K to 110 K.

became more pronounced after high annealing temperatures. Also, the I–V characteristics change their behavior, e.g. the pad current at low bias voltages became approximately zero while the current of the guard ring became large at zero voltage and decreases with increasing bias voltage. However, such behavior does not appear on the p-spray diodes. These findings led to the speculation that surface effects occurring between the guard ring and the pad area might be responsible for the above mentioned observations.

In order to study such surface effects, the standard I–V setup was slightly modified compared to Fig. 1(c) and Fig. 1(d). While the guard ring was connected to ground via a voltage source, the pad was connected to a current meter. In addition, a second voltage source was connected to the backside of the diode (reverse bias V_{back}). With this setup, the current flow between the guard ring and the pad could be measured by varying the voltage of the guard ring in the range from −1 V to +1 V. At the same time, a reverse voltage was applied on the backside. All the conductance measurements were performed at 20 °C and humidity below 10% (Similar to the I–V/C–V setup). As an example, Fig. 15 presents such surface I–V curves at a constant V_{back} = 10 V for several p-stop diodes irradiated to different dose values.

The slope of the surface current in the linear range (−0.5 V to + 0.5 V) provides the surface conductance G, given by:

$$G = \frac{dI}{dV} \tag{10}$$

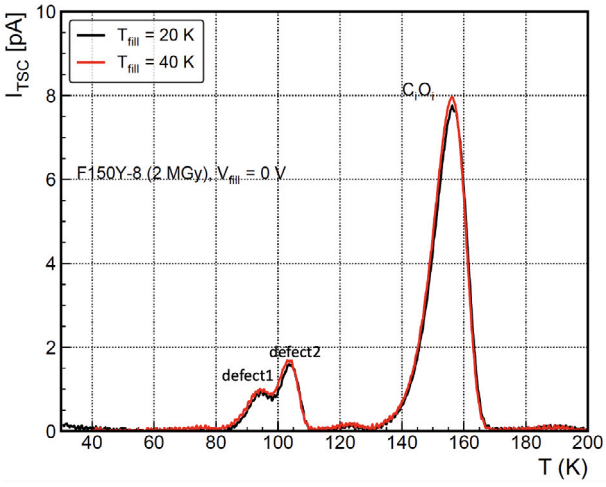

Fig. 14. 0 V injection performed on diode F150P-8 after isochronal annealing at T_{ann} = 300 °C. Measurement details: T_{fill} = 20 and 40 K.

Fig. 16 demonstrates the dependence of the conductance G versus V_{back}. The decrease of G with increasing V_{back} indicates a decrease in the charge carrier concentration near the surface. For $V_{back} \geq$ 50 V

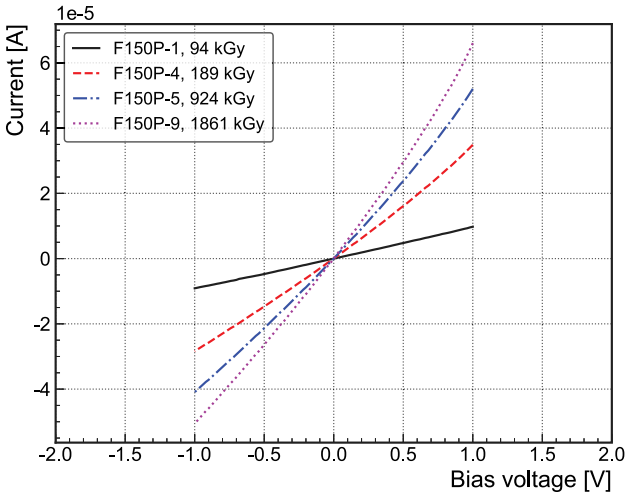

Fig. 15. Current measured on the pad with varying the bias on the guard from −1 V to 1 V for *p*-stop diodes with different irradiation dose values, V_{back} = −10 V.

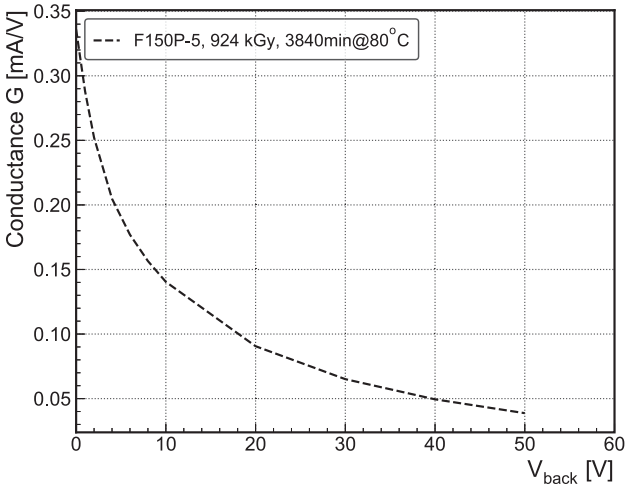

Fig. 16. Conductance G developed with bias on the backside while grounding the guard ring.

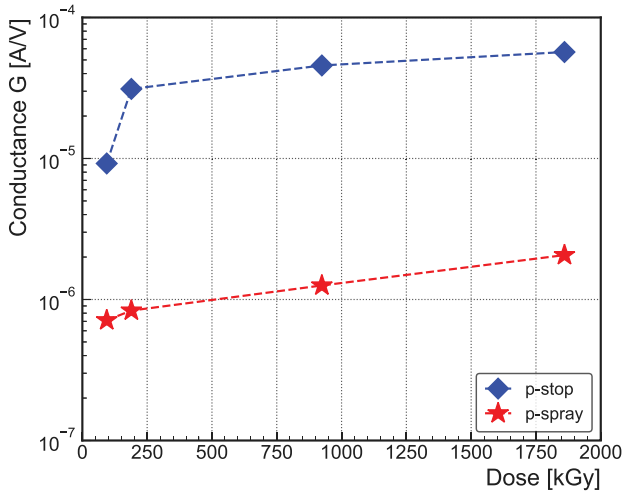

Fig. 17. The development of G with dose, V_{back} = −10 V.

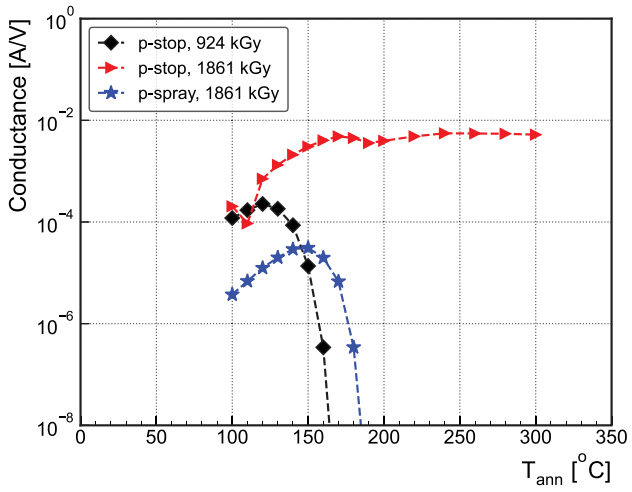

Fig. 18. Development of surface conductance with T_{ann} at backside applied −10 V.

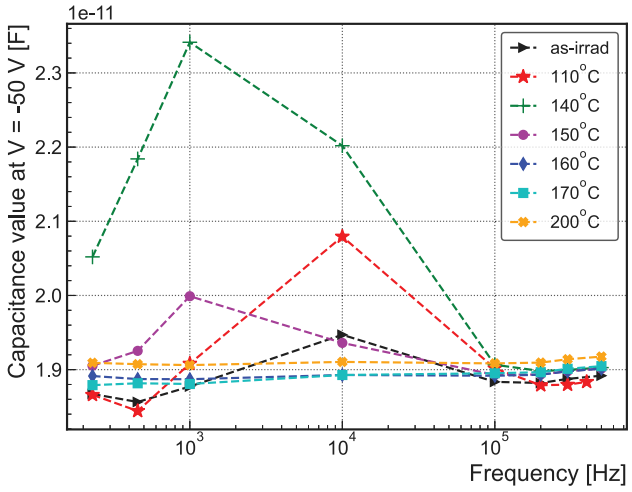

Fig. 19. Capacitance value when applied V = −50 V vs. frequency developed with annealing for *p*-stop after irradiation with D = 924 kGy.

the diode F150P-5 irradiated to 0.924 MGy becomes fully depleted. The dose dependence of the surface conductance is plotted in Fig. 17, for both, *p*-stop and *p*-spray diodes. There is more than one order of magnitude difference between the G values in the two types of diodes. This indicates that a much larger interface trap concentration exists in the *p*-stop diodes compared to the *p*-spray ones.

Isochronal annealing studies were performed for two *p*-stop diodes (F150P-7 (0.924 MGy), F150P-8 (1.861 MGy)) and one *p*-spray diode (F150Y-8 (1.861 MGy)).

The dependence of G on the annealing temperature T_{ann} is shown in Fig. 18. For the 924 kGy irradiated diodes, the changes in G are observed first as an increase for annealing up to 120 °C, followed by a rapid decrease with increasing T_{ann}. At the same time, after the 1864 kGy dose, the conductance of the *p*-stop sample is much larger than that of the *p*-spray one. On the other hand, in the highly irradiated *p*-stop device, G increases up to about 150 °C and stays thereafter nearly constant up to the end of the annealing experiment, at the temperature of 300 °C. A frequency dependence in C–V measurements is only observed if G is larger than 3×10^{-6} or 2×10^{-6} A/V at V_{back} = 10 or 50 V, respectively. The frequency dependencies of the capacitance measured after annealing at different temperatures on F150P-7 *p*-stop diode are shown in Fig. 19, in the 230 Hz to 500 kHz frequency range. The capacitance values are taken for a reverse bias of 50 V, which is

slightly below the full depletion voltage. As it can be seen, the maximal capacitance value is observed for T_{ann} = 140 °C and a frequency of 1 kHz. From 160 °C on, the frequency dependence vanishes, in accordance with the corresponding very low conductance shown in Fig. 18. It is worth noting that, above 100 kHz, the capacitance is constant for all the annealing temperatures. Measuring the capacitance in such a frequency-independent range is considered to be a safe procedure for performing the *C–V* measurements and extracting further the N_{eff} profiles. Under this assumption, the errors for all capacitance values at 500 kHz are below 4% for *p*-stop diodes with dose values below 1 MGy. Due to the increase of the conductance after 1.861 MGy doses, the capacitance of *p*-stop is not reliable anymore after annealing.

4. Conclusion

The radiation damage of two types of silicon diodes (*p*-spray and *p*-stop), manufactured on *p*-type Fz-material, with a resistivity of about 4 kΩ·cm and exposed to ^{60}Co γ-ray at different dose values (0.094 MGy, 0.189 MGy, 0.924 MGy, and 1.861 MGy) was investigated in this study. *I–V* and *C–V* measurements were employed for studying the radiation-induced changes in the density of leakage current (J_d) and in the effective space charge (N_{eff}). The results showed that with increasing the dose, N_{eff} decreases while J_d linearly increases, the latter exhibiting a similar trend to that of oxygen enriched *n*-type silicon irradiated with ^{60}Co γ-ray. In order to identify the γ-induced traps in the bulk of the samples, TSC measurements were performed on irradiated *p*-type diodes. The TSC spectra revealed the presence of defects, including H40K, VO, B_iO_i, C_iO_i, V_2, and the newly detected I_P^*. The results showed that all the concentrations of defects increased linearly with dose except the I_P^* that shows a quadratic dose dependence. DLTS technique has been employed for determining the trapping parameters of I_P^* (direct capture cross sections measurements and activation energy). The process of multi-phonon capture of holes by the C_iO_i defect was investigated by analyzing the corresponding TSC peak obtained after the filling of the defect was performed at different temperatures. The obtained results differ from those determined after irradiation with 1 MeV neutrons of *n*-type silicon diode, the capturing process on the C_iO_i defect being faster after irradiation with γ-rays. This is explained considering that there are additional potential barriers surrounding the disordered (clustered) regions produced by hadrons which slow down the charge transport in the diodes.

To gain a better understanding of the defects' thermal stability, kinetics and their impact on the device properties, isochronal annealing experiments were performed in the 100 °C to 300 °C temperature range. The TSC experiments revealed that C_iO_i complex is thermally stable up to the end of the isochronal annealing, performed up to 300 °C in our study. In contrast, the other radiation-induced defects change their concentrations during the thermal treatment. Thus, H40K anneals out at 120 °C while B_iO_i and I_P^* start to anneal out above 140 °C when the devices are recovering most of their initial doping. Two unidentified traps are detected to form during the annealing, labeled as *defect1* and *defect2*. *defect1* is forming during the treatment in the 140 °C–200 °C temperature range and transforms into *defect2* after annealing at higher temperatures. Both defects were found to be hole traps and neutrally charged at room temperature.

The results of the macroscopic measurements showed that the density of leakage current (J_d) measured in full depletion conditions (at $V = -300$ V) remains stable for annealing temperatures up to 200 °C, indicating that none of the annealed out defects has an influence on the measured current. In the 200 °C–300 °C temperature range of annealing, J_d increases up to 260 °C and then decreases. No evidence for bulk defects responsible for such behavior was detected in TSC experiments. Variations of N_{eff} were observed only in the 150 °C–200 °C annealing temperature range, where the dissociation of the B_iO_i defect occurs and N_{eff} increases because the initial removed substitutional Boron is recovered. Depending on the isolation technique used for the fabrication of the two types of investigated diodes, different frequency dependences were evidenced, according not only to the irradiation dose but also to the isolation technique used for separating the pad from the guard ring. To further investigate this phenomenon, surface conductance (*G*) measurements were performed on different samples. The frequency dependence in *C–V* measurements is only observed if *G* was larger than 3×10^{-6} or 2×10^{-6} A/V at V_{back} = 10 or 50 V, respectively. This is not the case for most of the irradiated *p*-spray diodes, apart from the highest dose of 1861 kGy in this study, after annealing at high temperature. For irradiated *p*-stop diodes, the value of *G* is consistently above this limit, but it can be decreased by annealing for dose values below 1 MGy (F150P-7).

CRediT authorship contribution statement

C. Liao: Data curation, Formal analysis, Investigation, Writing – original draft. **E. Fretwurst:** Writing – review & editing. **E. Garutti:** Writing – review & editing. **J. Schwandt:** Writing – review & editing. **I. Pintilie:** Writing – review & editing. **A. Nitescu:** Writing – review & editing. **A. Himmerlich:** Writing – review & editing. **M. Moll:** Writing – review & editing. **Y. Gurimskaya:** Writing – review & editing. **Z. Li:** Writing – review & editing.

Declaration of competing interest

The authors declare that they have no known competing financial interests or personal relationships that could have appeared to influence the work reported in this paper.

Data availability

No data was used for the research described in the article.

Acknowledgments

This work has been carried out in the framework of the RD50 Collaboration. The project has received funding from the European Unions Horizon 2020 Research and Innovation program under Grant Agreement no. 654168. C. Liao would like to thank the Deutsche Forschungsgemeinschaft (DFG, German Research Foundation) under Germany's Excellence Strategy – EXC2121 "Quantum Universe" – 390833306 and Professor Z. Li for supporting his stay at the University of Hamburg. I. Pintilie and A. Nitescu acknowledge the funding received through IFA-CERN-RO 8/2022 project. Z. Li acknowledges the funding received through the Key Scientific and Technological Innovation Project of Shandong Province under Grant No. 2019 TSLH 0316, and the project of Yantai Institute for the exchange of Driving Forces under Grants No. 2019XJDN002.

References

[1] G. Casse, P.P. Allport, S. Martíí Garcia, M. Lozano, P.R. Turner, Performances of miniature microstrip detectors made on oxygen enriched p-type substrates after very high proton irradiation, Nucl. Instrum. Methods Phys. Res. A 535 (1) (2004) 362–365, http://dx.doi.org/10.1016/j.nima.2004.07.153.

[2] M. Moll, et al., Development of radiation tolerant semiconductor detectors for the super-LHC, Nucl. Instrum. Methods Phys. Res. A 546 (1) (2005) 99–107, http://dx.doi.org/10.1016/j.nima.2004.07.153.

[3] G. Kramberger, et al., Radiation effects in low gain avalanche detectors after hadron irradiations, J. Instrum. 10 (7) (2015) P07006, http://dx.doi.org/10.1088/1748-0221/10/07/p07006.

[4] M. Ferrero, et al., Radiation resistant LGAD design, Nucl. Instrum. Methods Phys. Res. A 919 (2019) 16–26, http://dx.doi.org/10.1016/j.nima.2018.11.121.

[5] P.M. Mooney, L.J. Cheng, M. Süli, J.D. Gerson, J.W. Corbett, Defect energy levels in boron-doped silicon irradiated with 1-MeV electrons, Phys. Rev. B 15 (8) (1977) 3836–3843, http://dx.doi.org/10.1103/PhysRevB.15.3836.

[6] I. Pintilie, E. Fretwurst, G. Lindström, Cluster related hole trap with enhanced-field-emission the source for long term annealing in hadron irradiated Si diodes, Appl. Phys. Lett. 92 (2008) 024101, http://dx.doi.org/10.1063/1.2832646.

[7] M. Bruzzi, et al., Processing and first characterization of detectors made with high resistivity n- and p-type Czochralski silicon, Nucl. Instrum. Methods Phys. Res. A 522 (2005) 20–26, http://dx.doi.org/10.1016/j.nima.2005.06.001.

[8] I. Pintilie, G. Lindström, A. Junkes, E. Fretwurst, Radiation-induced point- and cluster-related defects with strong impact on damage properties of silicon detectors, Nucl. Instrum. Methods Phys. Res. A 611 (1) (2009) 52–68, http://dx.doi.org/10.1016/j.nima.2009.09.065.

[9] J. Coutinho, et al., Electronic and dynamical properties of the silicon trivacancy, Phys. Rev. B 86 (2012) 174101, http://dx.doi.org/10.1103/PhysRevB.86.174101.

[10] L.C. Kimerling, M.T. Asom, J.L. Benton, P.J. Drevinsky, C.E. Caefer, Interstitial defect reactions in silicon, in: Defects in Semiconductors 15, in: Materials Science Forum, vol. 38, 1989, pp. 141–150, http://dx.doi.org/10.4028/www.scientific.net/MSF.38-41.141.

[11] C. Möller, K. Lauer, Light-induced degradation in indium-doped silicon, Phys. Status Solidi RRL 7 (7) (2013) 461–464, http://dx.doi.org/10.1002/pssr.201307165.

[12] K. Lauer, et al., Activation energies of the In_{Si}-si_i defect transitions obtained by carrier lifetime measurements, Phys. Status Solidi C 14 (5) (2017) 1600033, http://dx.doi.org/10.1002/pssc.201600033.

[13] Y. Gurimskaya, et al., Radiation damage in p-type EPI silicon pad diodes irradiated with protons and neutrons, Nucl. Instrum. Methods Phys. Res. A. 958 (2020) 162221, http://dx.doi.org/10.1016/j.nima.2019.05.062.

[14] C. Liao, et al., The boron oxygen (B_iO_i) defect complex induced by irradiation with 23 GeV protons in p-type epitaxial silicon diodes, IEEE Trans. Nucl. Sci. 69 (3) (2022) 576–586, http://dx.doi.org/10.1109/TNS.2022.3148030.

[15] A. Himmerlich, et al., Defect characterization studies on neutron irradiated boron-doped silicon pad diodes and low gain avalanche detectors, Nucl. Instrum. Methods Phys. Res. A. 1048 (2023) 167977, http://dx.doi.org/10.1016/j.nima.2022.167977.

[16] C. Liao, et al., Investigation of the boron removal effect induced by 5.5 MeV electrons on highly doped EPI- and Cz-silicon, Nucl. Instrum. Methods Phys. Res. A. 1056 (2023) 168559, http://dx.doi.org/10.1016/j.nima.2023.168559.

[17] C. Besleaga, A. Kuncser, A. Nitescu, G. Kramberger, M. Moll, I. Pintilie, Bistability of the BiOi complex and its implications on evaluating the acceptor removal process in p-type silicon, Nucl. Instrum. Methods Phys. Res. A 1017 (2021) 165809, http://dx.doi.org/10.1016/j.nima.2021.165809.

[18] A. Himmerlich, et al., Defect characterization studies and modelling of defect spectra for 60co gamma-irradiated epitaxial p-type si diodes, in: Presented At the 41th RD50Workshop, Sevilla, Spain, 2022, [Online]. Available: https://indico.cern.ch/event/1132520/contributions/5141025/.

[19] C. Liao, et al., Investigation of high resistivity p-type FZ silicon diodes after ^{60}Co - gamma irradiation, in: Presented At the 40th RD50 Workshop, CERN, 2022, [Online]. Available: https://indico.cern.ch/event/1157463/.

[20] M. Mikestikova, Preliminary results of bulk damage study in gamma irradiated n-in-p silicon strip sensors, in: Presented At the 34th RD50 Workshop, Lancaster University, 2019, [Online]. Available: https://indico.cern.ch/event/812761/contributions/3459084/.

[21] J.H. Cahn, Irradiation damage in germanium and silicon due to electrons and Gamma rays, J. Appl. Phys. 30 (1956) 1310–1316, http://dx.doi.org/10.1063/1.1735310.

[22] M. Moll, Radiation Damage in Silicon Particle Detectors: Microscopic Defects and Macroscopic Properties (Ph.D. dissertation), Dept. Phys. Univ. Hamburg, Hamburg, Germany, 1999, DESY-THESIS-1999-040.

[23] https://www.hamamatsu.com/eu/en.html.

[24] The tracker group of the CMS collaboration, evaluation of HPK n^+-p planar pixel sensors for the CMS phase-2 upgrade, Nucl. Instrum. Methods Phys. Res. A. 1053 (2023) 168326, http://dx.doi.org/10.1016/j.nima.2023.168326.

[25] J. Schwandt, CMS pixel detector development for the HL-LHC, Nucl. Instrum. Methods Phys. Res. A. 924 (2019) 59–63, http://dx.doi.org/10.1016/j.nima.2018.08.121.

[26] M. Roguljic, A. Starodumov, A. Karadzhinova-Ferrer, D. Ferencek, A.A. Ahmed, L.M. Jara-Casas, Low Dose Rate ^{60}co Facility in Zagreb, PoS, Vol. Vertex2019, 2020, p. 066, http://dx.doi.org/10.22323/1.373.0066.

[27] I. Pintilie, L. Pintilie, M. Moll, E. Fretwurst, G. Lindström, Thermally stimulated current method applied on diodes with high concentration of deep trapping levels, Appl. Phys. Lett. 78 (2001) 550, http://dx.doi.org/10.1063/1.1335852.

[28] I. Pintilie, M. Buda, E. Fretwurst, G. Lindström, J. Stahl, Stable radiation-induced donor generation and its influence on the radiation tolerance of silicon diodes, Nucl. Instrum. Methods Phys. Res. A 556 (1) (2006) 197–208, http://dx.doi.org/10.1016/j.nima.2005.10.013.

[29] https://www.thermofisher.com/de/de/home/life-science/lab-equipment/lab-ovens-furnaces/lab-heating-drying-ovens.html.

[30] E. Fretwurst, et al., Bulk damage effects in standard and oxygen-enriched silicon detectors induced by ^{60}Co-gamma radiation, Nucl. Instrum. Methods Phys. Res. A 514 (1) (2003) 1–8, http://dx.doi.org/10.1016/j.nima.2003.08.077.

[31] I. Pintilie, E. Fretwurst, G. Lindström, J. Stahl, Results on defects induced by ^{60}Co gamma irradiation in standard and oxygen-enriched silicon, Nucl. Instrum. Methods Phys. Res. A 514 (1) (2003) 18–24, http://dx.doi.org/10.1016/j.nima.2003.08.079.

[32] E. Fretwurst, F. Hönniger, G. Kramberger, G. Lindström, I. Pintilie, R. Röder, Radiation damage studies on MCz and standard and oxygen enriched epitaxial silicon devices, Nucl. Instrum. Methods Phys. Res. A 583 (1) (2007) 58–63, http://dx.doi.org/10.1016/j.nima.2007.08.194.

[33] A. Hallén, N. Keskitalo, F. Masszi, V. Nágl, Lifetime in proton irradiated silicon, J. Appl. Phys. 79 (8) (1996) 3906–3914, http://dx.doi.org/10.1063/1.361816.

[34] I. Pintilie, E. Fretwurst, G. Lindström, J. Stahl, Close to midgap trapping level in ^{60}Co gamma irradiated silicon detectors, Appl. Phys. Lett. 81 (2002) 165–167, http://dx.doi.org/10.1063/1.1490397.

[35] I. Pintilie, E. Fretwurst, G. Lindström, J. Stahl, Second-order generation of point defects in gamma-irradiated float-zone silicon, an explanation for type inversion, Appl. Phys. Lett. 82 (13) (2003) 2169–2171, http://dx.doi.org/10.1063/1.1564869.

[36] I. Pintilie, E. Fretwurst, G. Kramberger, G. Lindström, Z. Li, J. Stahl, Second-order generation of point defects in highly irradiated float zone silicon-annealing studies, Physica B 340–342 (2003) 578–582, http://dx.doi.org/10.1016/j.physb.2003.09.131.

[37] H. Feick, Radiation Tolerance of Silicon Particle Detectors for High-Energy Physics Experiments (Ph.D. dissertation), Dept. Phys. Univ. Hamburg, Hamburg, Germany, 1997, DESY-F-35-D-97-8.

[38] C.T. Sah, L. Forbes, L.L. Rosier, A.F. Tasch, Thermal and optical emission and capture rates and cross sections of electrons and holes at imperfection centers in semiconductors from photo and dark junction current and capacitance experiments, Solid State Electron. 13 (6) (1970) 759–788, http://dx.doi.org/10.1016/0038-1101(70)90064-X.

[39] M.G. Buehler, Impurity centers in pn junctions determined from shifts in the thermally stimulated current and capacitance response with heating rate, Solid State Electron. 15 (1) (1972) 69–79, http://dx.doi.org/10.1016/0038-1101(72)90068-8.

[40] M.A. Green, Intrinsic concentration, effective densities of states, and effective mass in silicon, J. Appl. Phys. 67 (6) (1990) 2944–2954, http://dx.doi.org/10.1063/1.345414.

[41] R. Radu, I. Pintilie, L.C. Nistor, E. Fretwurst, G. Lindström, L.F. Makarenko, Investigation of point and extended defects in electron irradiated silicon dependence on the particle energy, J. Appl. Phys. 117 (2015) 164503, http://dx.doi.org/10.1063/1.4918924.

[42] S. Weiss, R. Kassing, Deep level transient Fourier spectroscopy (DLTFS) - A technique for the analysis of deep level properties, Solid-State Electron. 31 (12) (1988) 1733–1742, http://dx.doi.org/10.1016/0038-1101(88)90071-8.

[43] A. Chilingarov, Temperature dependence of the current generated in Si bulk, J. Instrum. 8 (10) (2013) P10003, http://dx.doi.org/10.1088/1748-0221/8/10/P10003.

[44] P. Bräunlich, Thermally Stimulated Relaxation in Silicon, Clarendon Press. section 2.5, 1979, Link: https://catalogue.nla.gov.au/Record/2253954.

[45] B.G. Svensson, B. Mohadjeri, A. Hallén, J.H. Svensson, J.W. Corbett, Divacancy acceptor levels in ion-irradiated silicon, Phys. Rev. B 43 (1991) 2292–2298, http://dx.doi.org/10.1103/PhysRevB.43.2292.

[46] E.V. Monakhov, J. Wong-Leung, A. Yu. Kuznetsov, C. Jagadish, B.G. Svensson, Ion mass effect on vacancy-related deep levels in Si induced by ion implantation, Phys. Rev. B 65 (9) (2002) 245201, http://dx.doi.org/10.1103/PhysRevB.65.245201.

[47] P.J. Drevinsky, C.E. Caefer, S.P. Tobin, J.C. Mikkelsen, L.C. Kimerling, Influence of oxygen and boron on defect production in irradiated silicon, Mater. Res. Soc. Symp. Proc. 104 (1988) 167–172, http://dx.doi.org/10.1557/PROC-104-167.

[48] O.V. Feklisova, N.A. Yarykin, J. Weber, Annealing kinetics of boron-containing centers in electron-irradiated silicon, Semiconductors 47 (2013) 228–231, http://dx.doi.org/10.1134/S1063782613020085.

[49] I. Mandić, et al., Gain recovery in heavily irradiated low gain avalanche detectors by high temperature annealing, Nucl. Instrum. Methods Phys. Res. A 1055 (2023) 168553, http://dx.doi.org/10.1016/j.nima.2023.168553.